

14. D. R. Rolison, *Science* **299**, 1698 (2003).
15. J. V. Ryan *et al.*, *Nature* **406**, 169 (2000).
16. D. R. Rolison, B. Dunn, *J. Mater. Chem.* **11**, 963 (2001).
17. T. Gacoin, K. Lahilil, P. Larregaray, J.-P. Boilot, *J. Phys. Chem. B* **105**, 10228 (2001).
18. 4-fluorophenylthiolate-capped nanoparticles of cubic CdS, CdSe, ZnS, and PbS were prepared by a modified literature synthesis (17) and dispersed in acetone to a concentration of ~0.05 to 0.5 M. Samples of 2 to 4 mL of the sols in polyethylene vials were treated with 0.1 to 0.2 mL of 3% H₂O₂ (CdS, ZnS, PbS) or 3% tetranitromethane (CdSe) to induce gelation. Gels were aged for several days to a week, exchanged multiple times with acetone, and dried in a SPI-Dry (Structure Probe, Inc., West Chester, PA) critical-point dryer using CO₂.
19. Materials and methods are available as supporting material on *Science* Online.
20. J. Aldana, Y. A. Wang, X. Peng, *J. Am. Chem. Soc.* **123**, 8844 (2001).
21. P. A. Webb, C. Orr, *Analytical Methods in Fine Particle Technology* (Micromeritics Instrument Corp., Norcross, GA, ed. 1, 1997).
22. Z. Zhang, T. J. Pinnavaia, *J. Am. Chem. Soc.* **124**, 12294 (2002).
23. A. H. Janssen, A. J. Koster, K. P. de Jong, *J. Phys. Chem. B* **106**, 11905 (2002).
24. W. Dong, D. R. Rolison, B. Dunn, *Electrochem. Solid State Lett.* **3**, 457 (2000).
25. J. W. Long, K. E. Swider-Lyons, R. M. Stroud, D. R. Rolison, *Electrochem. Solid-State Lett.* **3**, 453 (2000).
26. W.-W. So, J.-S. Jang, Y.-S. Rhee, K.-J. Kim, S.-J. Moon, *J. Coll. Inter. Sci.* **237**, 136 (2001).
27. C. B. Murray, D. J. Norris, M. G. Bawendi, *J. Am. Chem. Soc.* **115**, 8706 (1993).
28. Z. A. Peng, X. Peng, *J. Am. Chem. Soc.* **123**, 183 (2001).
29. M. L. Steigerwald, L. E. Brus, *Acc. Chem. Res.* **23**, 183 (1990).
30. Surface area (BET), 106 to 124 m²/g (mean 115 m²/g); adsorption average pore diameter (BJH), 23 to 28 nm; adsorption cumulative pore volume (BJH), 0.70 to 0.73 cm³/g.
31. Z. Tang, N. A. Kotov, M. Giersig, *Science* **297**, 237 (2002).
32. G. Reichenauer, G. W. Scherer, *J. Non-Cryst. Solids* **285**, 167 (2001).
33. Financial support was provided by NSF (IGERT award

DEG-9870720 and CAREER award DMR-0094273) and Research Corporation (Research Innovation Award-R10617). We thank M. Kanatzidis (Michigan State University) for the use of solid-state optical bandgap and luminescence equipment, C. Wauchope and J. Mansfield (University of Michigan) for assistance with TEM analyses, and S. L. Suib (University of Connecticut) for critical reading of this manuscript. The microscopy in this publication was performed in the University of Michigan Electron Microbeam Analysis Laboratory on a JEOL 2010EX (JEOL-USA, Peabody, MA) purchased under NSF grant DMR-9871177.

Supporting Online Material

www.sciencemag.org/cgi/content/full/307/5708/397/DC1

Materials and Methods

Figs. S1 to S4

References and Notes

19 October 2004; accepted 15 December 2004
10.1126/science.1106525

Deep-Ultraviolet Quantum Interference Metrology with Ultrashort Laser Pulses

Stefan Witte,* Roel Th. Zinkstok,* Wim Ubachs, Wim Hogervorst, Kjeld S. E. Eikema†

Precision spectroscopy at ultraviolet and shorter wavelengths has been hindered by the poor access of narrow-band lasers to that spectral region. We demonstrate high-accuracy quantum interference metrology on atomic transitions with the use of an amplified train of phase-controlled pulses from a femtosecond frequency comb laser. The peak power of these pulses allows for efficient harmonic upconversion, paving the way for extension of frequency comb metrology in atoms and ions to the extreme ultraviolet and soft x-ray spectral regions. A proof-of-principle experiment was performed on a deep-ultraviolet (2 × 212.55 nanometers) two-photon transition in krypton; relative to measurement with single nanosecond laser pulses, the accuracy of the absolute transition frequency and isotope shifts was improved by more than an order of magnitude.

In recent years, the invention of the femtosecond frequency comb laser (1–3) has brought about a revolution in metrology. A frequency comb acts as a bridge between the radio frequency (RF) domain (typically tens of MHz) and the optical frequency domain (typically hundreds of THz). Thus, in precision spectroscopy, the optical cycles of a continuous wave (CW) ultrastable laser can be phase-locked and counted directly with respect to an absolute frequency standard such as an atomic clock (4, 5). The resultant frequency measurements approach a precision of 1 part in 10¹⁵ in certain cases, potentially enabling the detection of possible drift in the fundamental constants (6, 7), among other quantum mechanical applications.

Laser Centre, Vrije Universiteit, De Boelelaan 1081, 1081 HV Amsterdam, Netherlands.

*These authors contributed equally to this work.

†To whom correspondence should be addressed.
E-mail: kjeld@nat.vu.nl

Here, we perform precision metrology without the use of a CW laser. Instead, an atomic transition is excited directly with amplified and frequency-converted pulses from a femtosecond frequency comb laser. As a result of quantum interference effects in the atomic excitation process, we can achieve an accuracy that is about six orders of magnitude higher than the optical bandwidth of the individual laser pulses.

The method used is related to Ramsey's principle of separated oscillatory fields (8), which probes the phase evolution of an atom in spatially separated interaction zones. This technique is widely used in the RF domain for atomic fountain clocks (9). By extension, in the optical domain, excitation can be performed by pulses separated in time (rather than in space) to maintain phase coherence between the excitation contributions. Several experiments have been performed to investigate Ramsey-type quantum interference fringes in the optical domain (10–14) and

phase-stable amplification of single pulses (15). Actual quantitative spectroscopy with phase-coherent oscillator pulses has been limited to a few relative frequency measurements on fine and hyperfine structure of atoms (13, 14, 16) and relative and absolute measurements on rubidium (17); absolute frequency measurements with amplified pulses have been frustrated by an unknown phase difference between the pulses or by limited resolution.

We generate powerful laser pulses with a precise phase relationship by amplifying a selected pulse train from a frequency comb laser. This amplified frequency comb can be used to measure absolute optical frequencies directly. The advantage of amplified laser pulses is that the high peak power allows for efficient frequency upconversion in crystals and gases. It has been shown that harmonic generation in gases can preserve the coherence properties of the driving laser pulse (18, 19). Therefore, the present experiment paves the way for precision metrology with frequency combs at optical frequencies that are very difficult or almost impossible to reach with CW lasers, such as vacuum-ultraviolet and even shorter wavelengths (e.g., x-rays). Possible applications are precision spectroscopy of hydrogen-like ions and helium to test quantum electrodynamics and nuclear size effects. The technique may also lead to more accurate atomic clocks that operate on resonances with ultrahigh frequencies.

In quantum interference metrology (Fig. 1), an atom is excited by a train of *N* phase-locked laser pulses separated by a time *T*. Assuming a two-level system, the resulting excited-state population after the pulse train can be written as

$$|b_N|^2 = \left| \sum_{n=1}^N a_n \exp[i(n-1)(\omega_0 T + \varphi)] \right|^2 \quad (1)$$

where φ is the phase difference between subsequent laser pulses, and a_n is the

excitation amplitude for the n th pulse. Thus, $|b_n|^2$ is a periodic function of both the pulse delay T and the phase difference φ . The resonance frequency ω_0 is encoded not just in the amplitude a_n , as with conventional spectroscopy, but also in the phase of the oscillating population signal. The first pulse creates an atomic superposition with a well-defined initial phase. The maxima of the excited-state population occur when subsequent laser pulses arrive in phase with this superposition. If the time delay and the pulse-to-pulse phase shift are known, the exact transition frequency can be derived from the position of these maxima. The more pulses are used, the narrower the resulting interference fringes. Therefore, multiple-level contributions can be resolved by the use of a sufficient number of pulses.

This method to measure the transition frequency is largely insensitive to the laser pulse spectral shape, which only influences the global signal amplitude. Therefore, spectral distortions of the laser pulses due to amplification or harmonic generation have little influence on the measurement, provided the distortion is identical from pulse to pulse. In contrast, traditional single-pulse spectroscopy is strongly affected by chirp (20, 21). However, the periodicity of the signal with respect to T leads to an inherent ambiguity in the determination of the transition frequency. This ambiguity can be resolved if a previous measurement with an accuracy much better than the repetition frequency exists; otherwise, the measurement can be repeated with different repetition rates, as shown below.

The frequency comb used in our experiment is based on a mode-locked Ti:sapphire oscillator. It emits 7-nJ pulses with a bandwidth (full width at half maximum) of ~ 90 nm, centered at 800 nm, and with an adjustable repetition rate between 60.9 and 79 MHz. For frequency accuracy, both the repetition rate and the phase of the pulses are locked to a Global Positioning System–disciplined Rb atomic clock (1, 2, 22, 23). An electro-optic modulator (EOM) is used to select up to three consecutive pulses from the mode-locked pulse train. These pulses are amplified in a six-pass Ti:sapphire nonsaturating amplifier to an energy of about 15 μ J per pulse (24). Spectral filtering is applied in the amplifier to limit the bandwidth of the amplified pulses to <0.5 nm. This filtering reduces the complexity of the signal, as only a single transition will be excited (see below). The amplification process gives rise to a small phase shift (~ 100 to 200 mrad) between the pulses, which is measured with a 1σ accuracy of 25 mrad ($<1/250$ of an optical cycle). These measurements are performed by placing the amplifier in one arm of a Mach-Zehnder interferometer and

recording spatial interferograms on a charge-coupled device (CCD) camera, from which this phase shift can be extracted (25).

To demonstrate the potential of high-frequency quantum interference metrology, we selected the $4p^6 \rightarrow 4p^55p[1/2]_0$ two-photon transition in krypton at a frequency of $\omega_0/2\pi = 2821$ THz. Because both the ground state and the excited state of this transition are $J = 0$ states, the atoms can be considered two-level systems. The required wavelength of 212.55 nm for the two-photon krypton resonance was obtained by fourth-harmonic generation of the amplifier output

at 850.2 nm through sequential frequency doubling in two beta-barium borate (BBO) crystals. The resultant 212.55-nm pulses (1.6 μ J) were focused in a highly collimated atomic beam of krypton (Fig. 2). The excited-state population was probed by a delayed 532-nm ionization pulse (1.5 mJ, 100 ps) from a Nd:yttrium-aluminum-garnet laser-amplifier system, and the experiment was repeated at 1 kHz.

The isotope shift and the absolute transition measurements described below can be influenced by a possible systematic Doppler shift as a result of nonperpendicular excitation. Therefore, all measurements were

Fig. 1. The principle of quantum interference metrology. An atom in the ground state $|g\rangle$ is resonantly excited by a broadband laser pulse. This pulse creates a coherent superposition of the ground state and the excited state, with an initial phase difference between the states determined by the laser pulse. After the initial excitation, the superposition will evolve freely with a phase velocity $\omega_0 = (E_e - E_g)/\hbar$, where $E_e - E_g$ is the energy difference between the states and \hbar is Planck's constant divided by 2π . After a time T , a second pulse with a controlled phase illuminates the atom, interfering with the atomic superposition. Depending on the phase and the time delay T , the total $|g\rangle \rightarrow |e\rangle$ excitation probability can be either enhanced (case A, red pulse) or suppressed (case B, blue pulse). By measuring the amplitude of the superposition (i.e., the population of the excited state) after the second pulse (with, e.g., an ionizing laser pulse), the energy difference between the states can be deduced.

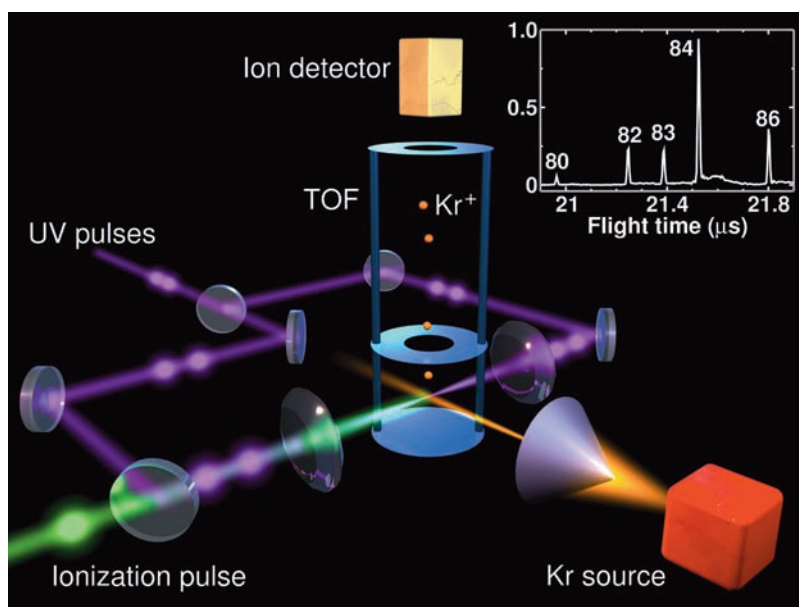
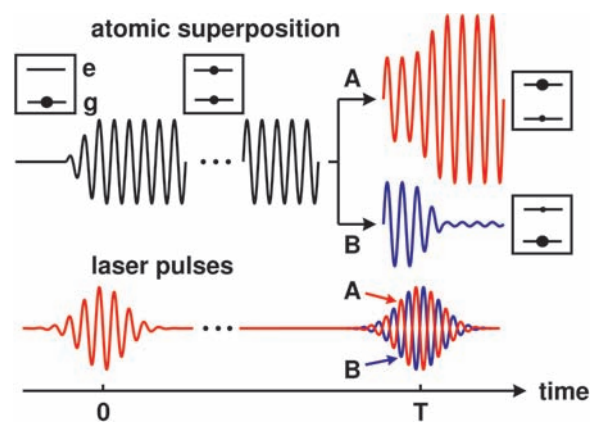


Fig. 2. Schematic of the experimental setup. The ultraviolet pulses (beam diameter 1 mm) are focused with an $f = 30$ cm lens in a collimated 0.3-mm-wide krypton beam (double skimmer arrangement, Doppler width <10 MHz) from both sides, crossing the beam perpendicularly. Measurements are performed with light from one side at a time. After the ultraviolet excitation, a delayed 532-nm pulse is used for ionization, and the resulting krypton ions are accelerated into a 60-cm time-of-flight mass spectrometer (TOF) by a pulsed electric field. Here the isotopes are separated in time (see inset) and counted with a channeltron detector.

performed from two opposite sides, with the average taken to determine the Doppler-free signal (26).

The data depend on the number of phase-locked pulses used to excite the transition (Fig. 3A). The pulse delay T was scanned by changing the comb laser repetition frequency, which is near 75 MHz. With a single pulse, the excitation probability is constant. With two pulses, a clear cosine oscillation is observed, with a contrast reaching 93%.

Three-pulse excitation gives the pulse-like structure predicted by Eq. 1 ($N = 3$) as well as an expected narrowing by 3/2 relative to two-pulse excitation. The solid lines are fits using Eq. 1, including an additional amplitude scaling factor to account for signal strength variations between the traces. In the three-pulse case, we took into account that the amplitude contribution of the pulses is not exactly equal because of spontaneous emission of the 5p state (lifetime 23 ns) and

differences in energy between the three pulses (27). For all other measurements, we used two-pulse excitation, as this minimizes the complexity of the experiment without sacrificing accuracy in this two-level case. The first of these measurements concerns the dependence on the pulse-to-pulse (carrier envelope) phase shift φ_{CE} (Fig. 3B), which is in complete agreement with expectations: The interference signal moves by one fringe when φ_{CE} of the comb laser is scanned through one-eighth of a cycle (due to the frequency conversion and two-photon transition).

Isotope shifts can be measured straightforwardly. The broad spectrum of the pulses places a frequency ruler on all isotopes simultaneously, so that spectra of ^{80}Kr through ^{86}Kr could be acquired at the same time (Fig. 3C). The measurements of Kaufman (28) were used for identification of the proper comb line for each isotope. The resulting shifts ($^{84}\text{Kr} - ^X\text{Kr}$), based on at least six measurements per isotope, are 302.02 ± 0.28 MHz (^{80}Kr), 152.41 ± 0.15 MHz (^{82}Kr), 98.54 ± 0.17 MHz (^{83}Kr), and -135.99 ± 0.17 MHz (^{86}Kr). The stated uncertainties (1σ) are smaller than the 6-MHz uncertainty reported by Kaufman (28) by a factor of 20 to 40.

In the measurement of the absolute transition frequency, an additional issue is the determination of the mode that corresponds to the true position of the resonance. The most accurate measurement to date (29) has an uncertainty of 45 MHz, which is not sufficient to assign the mode with confidence. Therefore, measurements were repeated at repetition rates near 60.9 MHz, 68.6 MHz, and 75.0 MHz to find the point at which the measurements coincide (four to nine measurements were performed at each repetition rate). After correction of the data for the phase shifts and systematic effects (30), there were three sets of possible positions for the 5p resonance transition (Fig. 4). The measurements have one clear coincidence (with an estimated probability of 98%, based on a statistical uncertainty of 2.5 MHz for each data point) near the literature value. Combining the three sets leads to an absolute frequency of 2,820,833,097.7 MHz with a 1σ uncertainty of 3.5 MHz (statistical and systematic errors combined), which is an order of magnitude smaller than the previous determination using single nanosecond laser pulses (29).

We envision several extensions of the above technique. One possibility is the use of a regenerative amplifier to amplify pulses to the μJ level at a repetition rate of 100 kHz. For high-frequency metrology, the resolution is ultimately limited by the comb laser and the interaction time of the atom with the pulses. This interaction time can be increased almost indefinitely if cooled ions in a trap are used in place of an atomic beam,

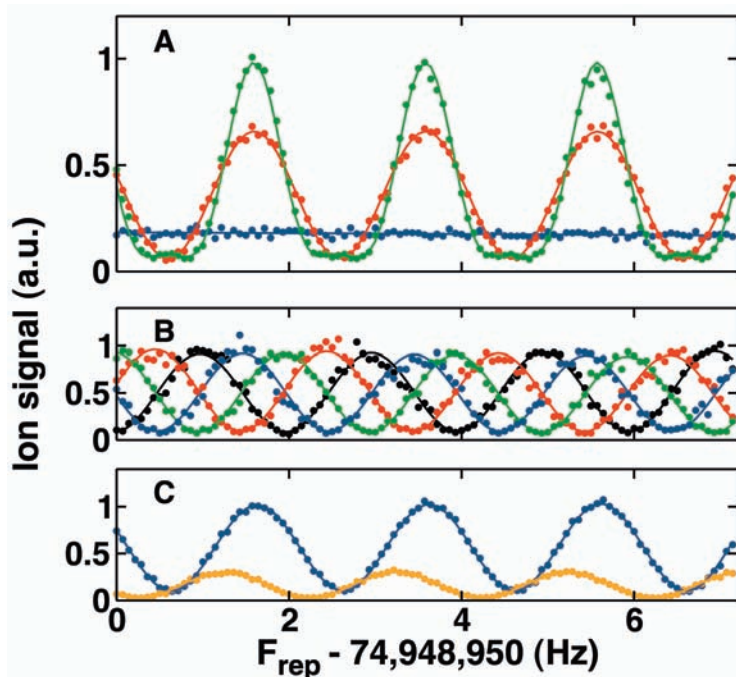
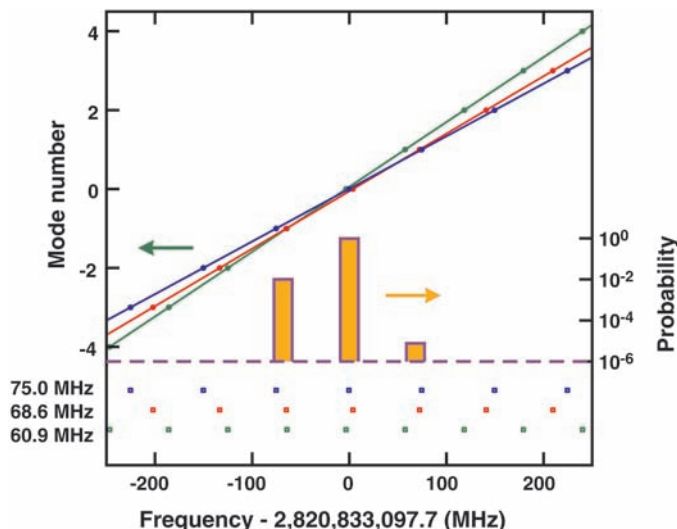


Fig. 3. Demonstration of quantum interference metrology. (A) ^{84}Kr signal as a function of the repetition rate of the comb laser for one (blue), two (red), and three (green) pulses 13.3 ns apart. The solid lines are fits to the theory (see text). (B) Measurement of the quantum interference signal for various phase differences between two excitation pulses, with the pulse-to-pulse phase shift (as seen by the atom) set to 0 (green), $\pi/2$ (blue), π (black), and $3\pi/2$ (red), respectively. (C) Measurement of the isotope shift between ^{84}Kr (blue trace) and ^{86}Kr (orange trace). The isotope shift can be determined from the phase shift between these two simultaneously recorded scans. The counter gate time is 10 s for each data point.

Fig. 4. Absolute calibration of the $4p^6 \rightarrow 4p^55p[1/2]_0$ transition in krypton is performed by finding the coincidence of three separate measurement series with repetition rates of 60.9 MHz (green), 68.6 MHz (red), and 75.0 MHz (blue). The orange bars (logarithmic scale) show the normalized statistical probability per mode for each measured mode position, revealing the location of the most probable coincidence.



opening the prospect of atomic optical clocks operating at vacuum-ultraviolet or extreme-ultraviolet frequencies. Outside frequency metrology, amplified frequency combs could be used to perform quantum control experiments on a time scale much longer than is currently possible, because phase coherence can be maintained for many consecutive laser pulses.

References and Notes

- R. Holzwarth *et al.*, *Phys. Rev. Lett.* **85**, 2264 (2000).
- D. J. Jones *et al.*, *Science* **288**, 635 (2000).
- Th. Udem, R. Holzwarth, T. W. Hänsch, *Nature* **416**, 233 (2002).
- M. Niering *et al.*, *Phys. Rev. Lett.* **84**, 5496 (2000).
- Th. Udem *et al.*, *Phys. Rev. Lett.* **86**, 4996 (2001).
- M. Fischer *et al.*, *Phys. Rev. Lett.* **92**, 230002 (2004).
- J. P. Uzan, *Rev. Mod. Phys.* **75**, 403 (2003).
- N. F. Ramsey, *Phys. Rev.* **76**, 996 (1949).
- A. Clairon, C. Salomon, S. Guellati, W. D. Phillips, *Europhys. Lett.* **16**, 165 (1991).
- M. M. Salour, C. Cohen-Tannoudji, *Phys. Rev. Lett.* **38**, 757 (1977).
- M. M. Salour, *Rev. Mod. Phys.* **50**, 667 (1978).
- R. Teets, J. N. Eckstein, T. W. Hänsch, *Phys. Rev. Lett.* **38**, 760 (1977).
- M. Bellini, A. Bartoli, T. W. Hänsch, *Opt. Lett.* **22**, 540 (1997).
- M. J. Snadden, A. S. Bell, E. Riis, A. I. Ferguson, *Opt. Commun.* **125**, 70 (1996).
- A. Baltuška *et al.*, *Nature* **421**, 611 (2003).
- J. N. Eckstein, A. I. Ferguson, T. W. Hänsch, *Phys. Rev. Lett.* **40**, 847 (1978).
- A. Marian, M. C. Stowe, J. R. Lawall, D. Felinto, J. Ye, *Science* **306**, 2063 (2004); published online 18 November 2004 (10.1126/science.1105660).
- R. Zerme *et al.*, *Phys. Rev. Lett.* **79**, 1006 (1997).
- S. Cavalieri, R. Eramo, M. Materazzi, C. Corsi, M. Bellini, *Phys. Rev. Lett.* **89**, 133002 (2002).
- K. S. E. Eikema, W. Ubachs, W. Vassen, W. Hogervorst, *Phys. Rev. A* **55**, 1866 (1997).
- S. D. Bergeson *et al.*, *Phys. Rev. Lett.* **80**, 3475 (1998).
- A. Apolonski *et al.*, *Phys. Rev. Lett.* **85**, 740 (2000).
- S. Witte, R. Th. Zinkstok, W. Hogervorst, K. S. E. Eikema, *Appl. Phys. B* **78**, 5 (2004).
- Standard amplifiers operate in saturated mode to reduce output power fluctuations and can therefore amplify only one pulse. In the present experiment, the number of pulses that can be amplified is limited to three by the EOM, which must be switched off before any backreflections from the amplifier lead to uncontrolled extra pulses. An additional Faraday isolator in the setup would lift this limitation.
- An EOM and polarizing optics were used to project the interference patterns for two consecutive pulses simultaneously and vertically displaced from one another on a CCD camera. The relative positions on the CCD (up or down) were alternated by switching the EOM; the relative phase shift to the comb laser was then determined by looking at the phase difference in both projection situations, so as to cancel out any alignment effects.
- The Doppler shift can in principle be reduced on a two-photon transition by measuring with colliding pulses from opposite sides. This arrangement also enhances the signal, as was seen experimentally. However, contrary to CW spectroscopy, Doppler-free signal (photons absorbed from opposite sides) and Doppler-shifted signal (two photons from one side) cannot be distinguished properly in the case of excitation with two ultrashort pulses, because the large bandwidth always contains a resonant frequency. This situation might lead to a calibration error when there is an imbalance in signal strength from opposite sides. Another aspect is that the total Doppler shift has an ambiguity due to the periodicity of the signal. The difference in Doppler shift for the isotopes, which is on the order of a few hundred kHz, therefore provides a valuable initial estimate of about 25 MHz for this shift. From the measurement

of the absolute positions, one can then determine the Doppler shift to be 29 MHz for each of the counterpropagating beams.

- The energy ratio of pulses 1, 2, and 3 is 1.0:0.91:0.6. In all measurements with two pulses, the pulse energies have been kept equal to within about 5%.
- V. Kaufman, *J. Res. Natl. Inst. Stand. Technol.* **98**, 717 (1993).
- F. Brandi, W. Hogervorst, W. Ubachs, *J. Phys. B* **35**, 1071 (2002).
- Two systematic effects dominate the determination of the resonance frequency: the phase shifts induced by the amplifier (100 to 200 mrad in the infrared), and the residual Doppler shift (2 MHz) due to possible misalignment of the counterpropagating beams. Other effects include light-shifts (0.47 ± 0.44 MHz), static field effects ($\ll 100$ kHz), the

second-order Doppler shift (~ 1 kHz), and a recoil shift (209 kHz). The phase shift due to the pulse-picker EOM is negligible (< 5 mrad) when it is aligned such that it acts as a pure polarization rotator, as verified experimentally. The phase shift due to frequency doubling is negligible as well, on the order of 1 mrad in the ultraviolet, as estimated from the model of (37).

- R. DeSalvo *et al.*, *Opt. Lett.* **17**, 28 (1992).
- Supported by the Foundation for Fundamental Research on Matter (FOM), the Netherlands Organization for Scientific Research (NWO), the EU Integrated Initiative FP6 program, and the Vrije Universiteit Amsterdam.

21 October 2004; accepted 30 November 2004
10.1126/science.1106612

Charging Effects on Bonding and Catalyzed Oxidation of CO on Au₈ Clusters on MgO

Bokwon Yoon,¹ Hannu Häkkinen,^{1*} Uzi Landman,^{1†} Anke S. Wörz,² Jean-Marie Antonietti,² Stéphane Abbet,² Ken Judai,² Ueli Heiz^{2†}

Gold octamers (Au₈) bound to oxygen-vacancy F-center defects on Mg(001) are the smallest clusters to catalyze the low-temperature oxidation of CO to CO₂, whereas clusters deposited on close-to-perfect magnesia surfaces remain chemically inert. Charging of the supported clusters plays a key role in promoting their chemical activity. Infrared measurements of the stretch vibration of CO adsorbed on mass-selected gold octamers soft-landed on MgO(001) with coadsorbed O₂ show a red shift on an F-center-rich surface with respect to the perfect surface. The experiments agree with quantum ab initio calculations that predict that a red shift of the C–O vibration should arise via electron back-donation to the CO antibonding orbital.

The exceptional catalytic properties of small gold aggregates (1, 2) have motivated research (3–17) aimed at providing insights into the molecular origins of this unexpected reactivity of gold. Investigations on size-selected small gold clusters, Au_n (2 ≤ n ≤ 20), soft-landed on a well-characterized metal oxide support [specifically, a MgO(001) surface with and without oxygen vacancies or F centers], revealed (4) that gold octamers bound to F centers of the magnesia surface are the smallest known gold heterogeneous catalysts that can oxidize CO into CO₂ at temperatures as low as 140 K. The same cluster bound to a MgO surface without oxygen vacancies is catalytically inactive for CO combustion (4).

Quantum-mechanical ab initio simulations, in juxtaposition with laboratory experiments,

led us to conclude (4, 5) that the key for low-temperature gold catalysis in CO oxidation is the binding of O₂ and CO to the supported gold nanocluster, which activates the O–O bond to a peroxo-like (or superoxo-like) adsorbate state. This process is enabled by resonances between the cluster's electronic states and the 2π* antibonding states of O₂, which are pulled below the Fermi level (E_F). Charging of the metal cluster, caused by partial transfer of charge from the substrate F center into the deposited cluster, underlies the catalytic activity of the gold octamers (Au₈), as well as that of other small gold clusters (Au_n, 8 ≤ n ≤ 20) (4). These investigations predicted that (i) the F centers on the metal oxide support surface play the role of active sites (a concept that has been central to the development of heterogeneous catalysis); (ii) these sites serve to anchor the deposited clusters more strongly than sites on the undefective surface (thus inhibiting their migration and coalescence); and, most important, (iii) these active sites control the charge state of the gold clusters, thus promoting the activation of adsorbed reactant molecules (that is, formation of the aforementioned peroxo or superoxo species) (18).

We have studied the cluster-charging propensity of the F-center active sites, both exper-

¹School of Physics, Georgia Institute of Technology, Atlanta, GA 30332–0430, USA. ²Departement Chemie, Lehrstuhl für Physikalische Chemie I, Technische Universität München, Lichtenbergstraße 4, 85747 Garching, Germany.

*Present address: Department of Physics, Nanoscience Center, Box 35, FIN-40014, University of Jyväskylä, Finland.

†To whom correspondence should be addressed. E-mail: uzi.landman@physics.gatech.edu (U.L.); ulrich.heiz@ch.tum.de (U.H.)